Optimized speckle variance OCT imaging of microvasculature

Adrian Mariampillai,[1] Michael K. K. Leung,[1] Mark Jarvi,[1] Beau A. Standish,[2] Kenneth Lee,[1] Brian C. Wilson,[1] Alex Vitkin,[1] and Victor X. D. Yang[2,*]

[1]*Department of Medical Biophysics, University of Toronto, Toronto, Ontario, Canada*
[2]*Department of Computer and Electrical Engineering, Ryerson University, Toronto, Ontario, Canada*
[*]*Corresponding author: yangv@ee.ryerson.ca*

Received December 15, 2009; revised February 5, 2010; accepted February 8, 2010; posted March 5, 2010 (Doc. ID 121509); published April 15, 2010

We optimize speckle variance optical coherence tomography (svOCT) imaging of microvasculature in high and low bulk tissue motion scenarios. To achieve a significant level of image contrast, frame rates must be optimized such that tissue displacement between frames is less than the beam radius. We demonstrate that higher accuracy estimates of speckle variance can enhance the detection of capillaries. These findings are illustrated *in vivo* by imaging the dorsal window chamber model (low bulk motion). We also show svOCT imaging of the nonstabilized finger (high bulk motion), using optimized imaging parameters, demonstrating better vessel detection than Doppler OCT.

OCIS codes: 110.4500, 170.3880, 170.4500, 170.2655.

Over the past decade, two types of algorithms and techniques for microvascular imaging using optical coherence tomography (OCT) have been developed, those that quantify blood flow/velocity, and those that visualize microvasculature but generally provide no quantitative flow information. Techniques in the first category, such as color Doppler imaging, are based on measuring phase shifts induced by moving scatterers [1–3]. In addition, Barton *et al.* have shown that speckle spatial frequency analysis in OCT intensity images can extract flow rates [4]. The second category was developed to visualize, but not quantify, microvascular flow. They include speckle variance (SV) [5] and power doppler OCT imaging [2,6]. Unlike the spatial frequency analysis method [4], speckle variance OCT (svOCT) identifies microvasculature by calculating the interframe intensity variance of structural images, where contrast is based on different time-varying properties of fluid (blood) versus solid tissue components. Despite promising results [5], interframe calculation is seriously affected by bulk tissue motion (BTM) if care is not taken to optimize acquisition parameters. In this Letter, we characterize svOCT image acquisition parameters under the two different bulk sample motion regimes in phantoms and then use these results to perform optimized svOCT in two corresponding *in vivo* imaging scenarios.

SV is calculated from the structural OCT signal by

$$SV_{ijk} = \frac{1}{N}\sum_{i=1}^{N}\left(I_{ijk} - \frac{1}{N}\sum_{i=1}^{N} I_{ijk}\right)^2, \quad (1)$$

where the gate length specifies the number of frames used in the variance calculation [N in Eq. (1)], and i, j, and k are indices for the frame, transverse, and axial pixels, respectively. Two parameters must be chosen to optimize the SV calculation in different tissue motion situations—the gate length N and frame rate or field of view. To determine these parameters we performed a phantom study using intralipid solution and a solid silicone gel containing titanium dioxide.

SV contrast is due to different time dependent scattering properties of fluids and solids. In the regime of complete decorrelation, when the time between acquired frames is large, the intensity values of a pixel within a fluid are Rayleigh distributed, whereas the intensity values of a pixel within a stationary solid are Gaussian distributed in time [7]. This leads to a difference in the magnitude of calculated variance and is the source of contrast between solids and fluids. For typical imaging speeds of 20–100 frames per second, we have previously demonstrated that complete decorrelation occurs between frames, even for stationary intralipid solution [5]. Furthermore, the contrast between solids and fluids is also affected by the accuracy of the variance estimate for these distributions. We define the SV signal-to-noise ratio (SNR) between a "fluid" pixel and a "solid" pixel, both with equal time averaged intensity I_0 as

$$SV_{SNR}(N,I_0) = \frac{SV_{Fluid}(N,I_0) - SV_{Solid}(N,I_0)}{\sqrt{\sigma^2_{Fluid}(N,I_0) + \sigma^2_{Solid}(N,I_0)}}, \quad (2)$$

where SV_{Fluid} and SV_{Solid} are the raw SV calculated from Eq. (1) and σ^2_{Fluid} and σ^2_{Solid} are the variances of SV_{Fluid} and SV_{Solid}, respectively.

To determine the optimal gate length in situations where BTM is low, the stationary solid gel and 10% stationary liquid intralipid solution were imaged using gate lengths of N=2, 4, 8, 16, and 32 at a single B-mode imaging plane. All experiments used a 36 kHz swept source OCT system similar to that described previously [5]. Briefly the system utilized a swept laser source based on a polygon filter configuration with coherence length of 6 mm. The axial imaging range was 3 mm and transverse imaging parameters were 800 A-scans over a 5-mm-wide region (160 A-scans/mm) using an NA=0.06 objective with beam radius ω_0=6.5 μm. The SV contrast SNR was

calculated over 1000 pixels. The intralipid exhibited an increase in SV SNR as a function of structural signal SNR and gate length, albeit with diminishing returns at larger N [Fig. 1(a)]. Therefore in this low-motion scenario, a long gate length ($N=8-32$) should be used.

However, a large amount of averaging is not feasible with high BTM. To simulate increasing BTM, we induced a transverse step between each B-mode frame used in the variance calculation, while scanning the solid stationary gel (160 A-scans/mm). The mean SV for intralipid and for the solid target with induced transverse steps of 1 to 25 μm between frames was calculated from 10×600 pixels regions with approximately equal mean SNR values using $N=2$ [Fig. 1(b)]. For an increased step size, diminishing contrast between the stationary gel and the intralipid target was observed, with a 50% decrease in variance at a displacement corresponding to the beam waist radius (~6.5 μm). The results were compared to a theoretical model used to describe decorrelation resulting from beam movement [8,9]. The SV data was fit to the function, $\mathrm{SV}\propto 1\text{-}\exp\left[-\frac{1}{2}\times(dx/\omega_o)^2\right]$, where dx is the step displacement (ranged from 1–25 μm). The results were in good agreement with the theoretical model at large displacements, and at small displacements the dominant contribution to the SV was from white noise. To account for these effects, the white noise ($\sigma^2_{\mathrm{white}}$) was measured in a region near the bottom of the image.

The correct choice of svOCT imaging parameters is thus crucial, and was demonstrated in two corresponding *in vivo* models: the dorsal window chamber model (low BTM) and the human nail root (high BTM). All animal procedures were performed under ketamine–xylazine anesthetic and approved by the Princess Margaret Hospital Animal Care Committee. In the first scenario, we used the dorsal window chamber model in a NCrNu (Taconic) female nude mice [5]. 1600 positions over a 5×5 mm^2 region were recorded; for each position, a gate of $N=8$ images with 800 A-scans per frame was used to keep the imaging time under 10 min, while maintaining good SV SNR. Confocal fluorescence microscopy (CFM) was performed as a comparison. CFM imaging (LSM 510 MetaNLO, Zeiss) was performed immediately after intravenous injection of 5 mg kg^{-1} of 500 kD fluorescein-labeled dextran. A $5\times$(NA=0.25) objective was used for imaging the 5×5 mm^2 region of the window chamber, from which a z stack of 10 images was acquired. Each imaged x-y section had a 40 μm depth of focus at a step size of 20 μm. The resultant projection (over 220 μm depth) images are shown in Figs. 2(a) and 2(b), with magnified regions demonstrated in Figs. 2(c) and 2(d), respectively. It is apparent that the SV technique can detect the capillaries, a significant improvement over our previously published work [5] due to the use of improved scanning pattern and $N=8$ gate length (previously, a continuously scanned high density three-dimensional (3D) image stack was used with $N=3$). The contrast of the smaller vessels in the svOCT image is lower than in the CFM image, but still clearly detectable. However, the capillaries in svOCT image appear blurred due to the transverse resolution of the system (~13 μm), as we chose to sacrifice transverse resolution for a larger depth of field. To further demonstrate the benefits of optimized svOCT imaging parameters, a 9L gliosarcoma tumor was imaged 9 days after implantation in the window chamber. Orthogonal slices through the structural data are shown in Fig. 3(a). The corresponding SV vascular map is shown in Fig. 3(b), where the vasculature has been color coded according to its depth in the tissue [10]. Satellite metastasis, not obvious in the structural image, are detected in the svOCT image [indicated by blue arrows in Fig. 3(b)]. Figures 3(c)–3(e) demonstrate how the contrast of smaller vessels improves as the gate length is increased from 2 to 8. Although the amount of data acquired to generate the image in Fig. 3(b) is large, it is significantly less than the storage requirements for phase sensitive techniques such as intensity modulated phase variance [10] and optical angiography [11].

To test the performance of SV in a high motion *in*

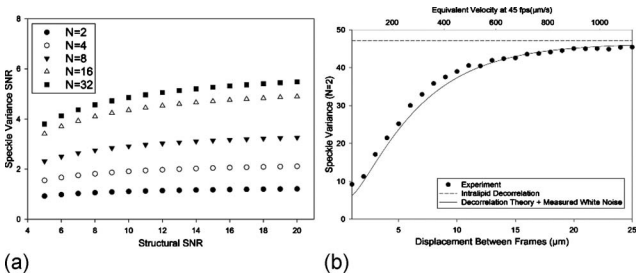

Fig. 1. (a) SV SNR measured from intralipid and silicone gel phantoms doped with titanium dioxide for various temporal averaging gates ($N=2,4,8,16,32$). (b) SV measured from intralipid compared to the silicone phantom demonstrating the effect of spatial shifts between frames ($N=2$) and theory.

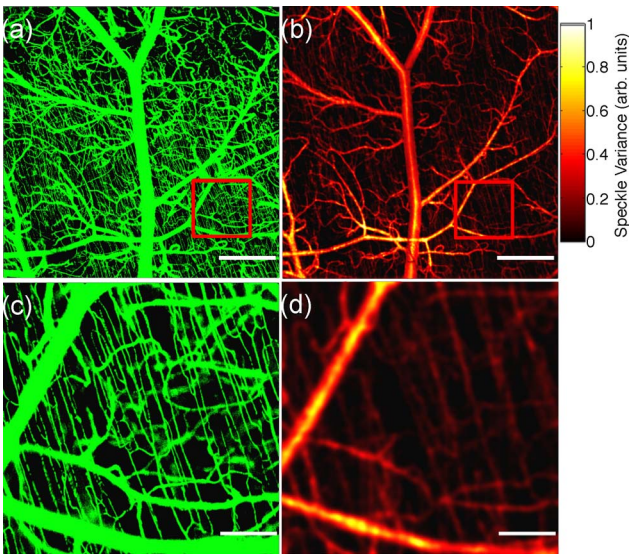

Fig. 2. (Color online) *In vivo* imaging in a low BTM situation: (a) fluorescence image; (b) corresponding SV image with gate length $N=8$; (c) magnified region of interest from fluorescence data; (d) magnified region of interest from SV data. Scale bars represent 1 mm in (a) and (b) and 200 μm in (c) and (d).

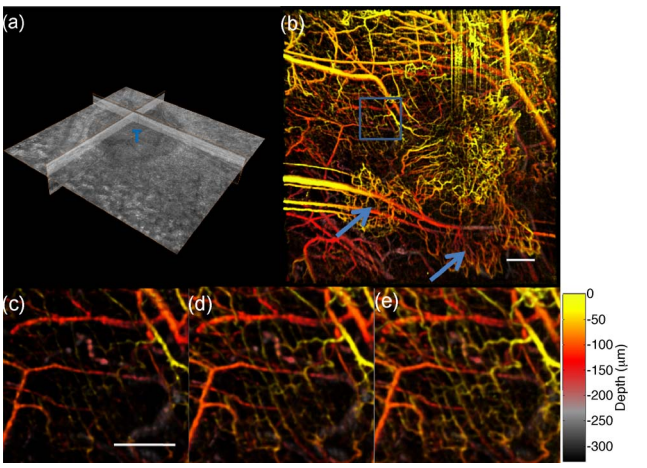

Fig. 3. (Color online) (a) Orthogonal slices through a 9L gliosarcoma tumor (t) implanted within the window chamber, with the main tumor appearing as the low intensity region. (b) Corresponding microvascular projection image for the tumor, with gate length $N=8$, arrows indicate the location of satellite metastasis. The color indicates relative depth of the vessels, with brighter shades indicating superficial (closest to the coverslip of the window chamber) and gray indicating deeply seated vasculature. (c)–(e) Magnified region (750×750 μm^2) demonstrating the effects of increased gate length ($N=2,4,8$). Scale is bar$=250$ μm.

vivo scenario, we imaged the vasculature in the nonstabilized human nail root [Fig. 4(a)]. In this situation we performed only B-mode imaging. Using a frame rate of 100 fps and $N=2$ gate length, minimized the tissue motion between frames to less than the beam radius, but structural features were present when using this short gate length. To improve the image, we averaged three consecutive SV images and displayed this result on the structural image shown in Fig. 4(a). We also compare the svOCT to color Doppler image processing [Fig. 4(b)].

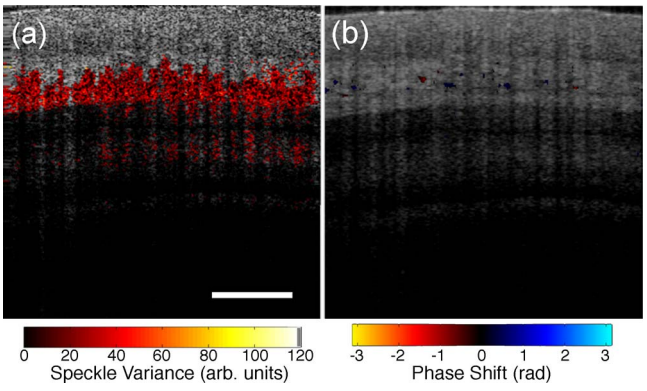

Fig. 4. (Color online) *In vivo* imaging in a high BTM situation: (a) structural image of human nail root with SV data overlay (Media 1), (b) structural image from the same location with color Doppler image overlay. (The scan head was tilted by 10° relative to the surface of the finger, providing a Doppler angle of ~80°.) (Media 2) Field of view is 2×2 mm^2. Scale bar$=500$ μm.

The Kasai velocity estimator was used with an ensemble length of 16, along with histogram rejection to remove BTM artifacts [2]. The SV approach is superior for detecting microvasculature when compared to color Doppler, due to its sensitivity and angle independence; however, it suffers from blood vessel shadowing artifacts [12,13].

To summarize, svOCT is a highly sensitive endogenous-contrast microvascular imaging technique that performs best in situations with low tissue motion, where large gate lengths can be used. Optimization of svOCT imaging parameters led to a significant improvement in capillary detection. In situations where tissue motion is high, the field of view or frame rate during acquisition must be optimized to keep inter-frame displacements to less than the beam waist radius. Finally, the lower computational complexity and data storage requirements of svOCT, relative to phase sensitive microvascular imaging techniques adds further utility to the technique.

This research was supported by the Natural Science and Engineering Research Council of Canada, Canadian Foundation for Innovation, the Canadian Institutes of Health Research, and Cancer Imaging Network Ontario.

References

1. S. Yazdanfar, M. Kulkarni, and J. Izatt, Opt. Express **1**, 424 (1997).
2. V. X. D. Yang, M. Gordon, B. Qi, J. Pekar, S. Lo, E. Seng-Yue, A. Mok, B. Wilson, and I. Vitkin, Opt. Express **11**, 794 (2003).
3. B. Vakoc, S. Yun, J. de Boer, G. Tearney, and B. Bouma, Opt. Express **13**, 5483 (2005).
4. J. Barton and S. Stromski, Opt. Express **13**, 5234 (2005).
5. A. Mariampillai, B. A. Standish, E. H. Moriyama, M. Khurana, N. R. Munce, M. K. K. Leung, J. Jiang, A. Cable, B. C. Wilson, I. A. Vitkin, and V. X. D. Yang, Opt. Lett. **33**, 1530 (2008).
6. Z. Ding, Y. Zhao, H. Ren, J. S. Nelson, and Z. Chen, Opt. Express **10**, 236 (2002).
7. J. W. Goodman, *Statistical Optics* (Wiley-Interscience, 2000).
8. V. X. D. Yang, A. Needles, D. Vray, S. Lo, B. C. Wilson, and S. Foster, Proc.-IEEE Ultrason. Symp. **1**, 453 (2004).
9. B. H. Park, M. C. Pierce, B. Cense, S. H. Yun, M. Mujat, G. J. Tearney, B. E. Bouma, and J. F. de Boer, Opt. Express **13**, 3931 (2005).
10. B. J. Vakoc, R. M. Lanning, J. A. Tyrrell, T. P. Padera, L. A. Bartlett, T. Stylianopoulos, L. L. Munn, G. J. Tearney, D. Fukumura, R. K. Jain, and B. E. Bouma, Nat. Med. **15**, 1219 (2009).
11. R. K. Wang, S. L. Jacques, Z. Ma, S. Hurst, S. R. Hanson, and A. Gruber, Opt. Express **15**, 4083 (2007).
12. V. J. Srinivasan, J. Y. Jiang, M. A. Yaseen, H. Radhakrishnan, W. Wu, S. Barry, A. E. Cable, and D. A. Boas, Opt. Lett. **35**, 43 (2010).
13. J. Fingler, R. J. Zawadzki, J. S. Werner, D. Schwartz, and S. E. Fraser, Opt. Express **17**, 22190 (2009).